SCIENTIFIC REPORTS

OPEN

Strain Engineering to Modify the Electrochemistry of Energy Storage Electrodes

Received: 06 April 2016
Accepted: 19 May 2016
Published: 10 June 2016

Nitin Muralidharan[1,2], Rachel Carter[2], Landon Oakes[1,2], Adam P. Cohn[2] & Cary L. Pint[1,2]

Strain engineering has been a critical aspect of device design in semiconductor manufacturing for the past decade, but remains relatively unexplored for other applications, such as energy storage. Using mechanical strain as an input parameter to modulate electrochemical potentials of metal oxides opens new opportunities intersecting fields of electrochemistry and mechanics. Here we demonstrate that less than 0.1% strain on a Ni-Ti-O based metal-oxide formed on superelastic shape memory NiTi alloys leads to anodic and cathodic peak potential shifts by up to ~30 mV in an electrochemical cell. Moreover, using the superelastic properties of NiTi to enable strain recovery also recovers the electrochemical potential of the metal oxide, providing mechanistic evidence of strain-modified electrochemistry. These results indicate that mechanical energy can be coupled with electrochemical systems to efficiently design and optimize a new class of strain-modulated energy storage materials.

Traditional routes to design materials for electrochemical applications require modification of material chemical composition to control reduction-oxidation energetics when coupled with an electrolyte[1,2]. This causes the search for improved nanomaterials in electrochemical applications to be driven by discovery-focused nanomaterial synthesis and fabrication. Due to the complex cooperative nature of energy storage device performance based on the pairing of electrodes and electrolytes, such routes rarely lead to new materials with characteristics, such as operating voltage, that outperform existing materials. Further, whereas computational guidance has brought about a new paradigm to predict targeted material compounds that can improve advanced energy storage systems[3,4], experimentalists often remain challenged by the synthesis process of such compounds, many of which are not naturally occurring. This presents a fundamental bottleneck in the conventional approach in which electrochemistry-oriented material research and development occurs that limits the rate of industry innovation in energy storage (and conversion) systems.

Strain engineering, a concept widely implemented in semiconductor electronics[5,6], opens new opportunities to engineer materials for electrochemical systems. The six-dimensional parameter space of the strain tensor[7] enables a nanostructure with a fixed chemical composition to have electronic and physical properties finely modulated in a manner that is virtually impossible to replicate by varying chemical composition. Unlike bulk materials, many nanostructures exhibit sizes where strain can homogenously propagate throughout the whole material, instead of only on a surface or an interface[6,8–14]. In this spirit, recent efforts have demonstrated the capability of strain in nanostructures to modify the energy landscape of catalytic and electro-catalytic surface-bound reactions[15–19] and modify oxygen ion diffusion in fuel cell technology[20–22]. The direct controlled correlation between mechanical strain as an input parameter and electrochemical processes in nanostructures for energy harvesting applications has only very recently been reported[23].

In the specific case of energy storage electrodes such as pseudocapacitors and batteries[1,24], Faradaic reactions especially in metal oxides induce a change to the oxidation state of the active material often regulated by the physical characteristics of the lattice structure to enable insertion or alloying of an ion species. Focus of current research efforts so far have been on the adverse effects of strain arising from the changes to the host lattice structures during electrochemical cycling of energy storage electrodes[25–27]. In this regard, mechanical strain imposed onto a nanostructure leading to both physical and electronic changes that can synergistically influence energy storage redox reactions has not yet been reported despite significant advances in the ability to produce, image, and understand strain effects in materials[15,28], especially those related to semiconductor electronics. Theoretical

[1]Interdisciplinary Materials Science Program, Vanderbilt University, Nashville, TN 37235 USA. [2]Department of Mechanical Engineering, Vanderbilt University, Nashville, TN 37235 USA. Correspondence and requests for materials should be addressed to C.L.P. (email: cary.l.pint@vanderbilt.edu)

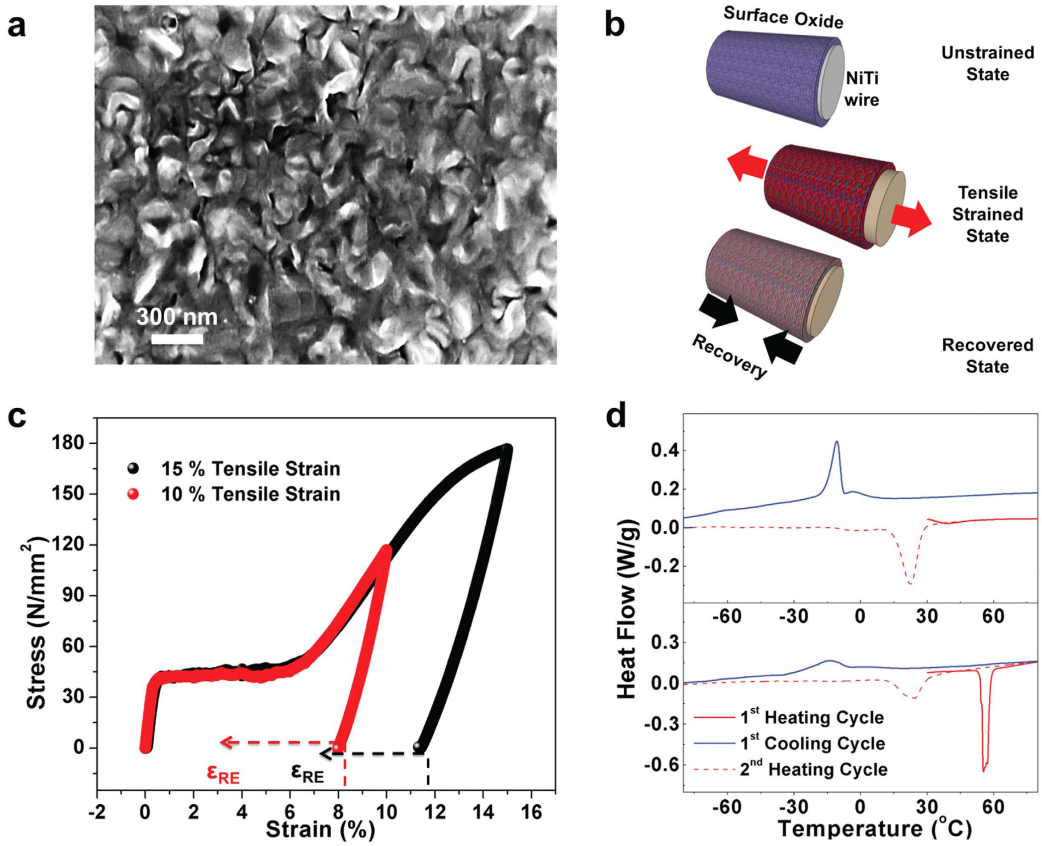

Figure 1. Strain engineering the surface oxide using NiTi alloy. (**a**) SEM image of the active NiO-TiO_2 based metal oxide formed on the surface of the NiTi alloy. (**b**) Schematic illustration of experimental system, including the application of strain and strain recovery on a NiTi wire with surface-bound active material. (**c**) Stress-strain behavior of the NiTi superelastic alloy deformed up to 10% and 15% tensile strain. The dashed lines and ε_{RE} indicates the heat assisted transformation process and the recovered strain respectively. (**d**) DSC thermograms of the unstrained (0%) and the tensile strained (15%) states. Red (line and dots) represents the heating cycle and blue line represents the cooling cycles.

studies have recently highlighted the prospect of pre-straining materials[29] even though experimental efforts in this direction remain elusive.

Here we demonstrate a study where nanostructured metal oxide materials are synthesized directly on the surface of a superelastic/shapememory NiTi wire. Under the application of strain to the NiTi and transferred to the surface-bound oxides, we observe consistent shifts in the anodic and cathodic potentials. By recovering this imposed strain, we observe consistent recovery of the electrochemical potentials, clearly demonstrating that strain, as opposed to other effects, is modulating the shifts in electrochemical potentials and can be a viable tool for the design of energy storage materials.

Metal-oxide nanostructures on superelastic NiTi

A Ni-Ti-O based oxide was grown on NiTi superelastic wires at 600 °C comprising of a mixed NiO-TiO_2 layer formed on top of a titanate layer on the surface of the NiTi material[30,31]. EDS maps (supporting information) obtained from the surface of the wire indicated a mixed Ni-Ti-O based surface oxide. Scanning electron microscopy (SEM) (Fig. 1a) was performed on the nanostructured surface oxides formed on the wire. To study strain-related modifications to energy storage processes, NiTi wires were tensile deformed to 10% and 15% strain at room temperature using an Instron mechanical testing system, with a corresponding small percentage of this input strain (less than 1%) transferred to the surface-bound oxide nanomaterial. The strained and unstrained wires with the mixed oxide layers were sonicated in peroxide at room temperature to impart nanotexturing to the oxide. This leads to a material architecture where nanostructured petals of NiO-TiO_2-based metal oxides are conformally coated on the surface of a NiTi wire in a seamless manner (Fig. 1b). The Ni-Ti-O surface metal oxide was further examined through Transmission electron microscopy (TEM) (supporting information, Figure S5) indicating the crystalline nanostructure of the surface oxide. The presence of the constituent elements of the nanostructured oxide (nickel, titanium, and oxygen) was further verified using STEM EDS maps. This architecture is ideally suited to correlate strain as an input parameter to the NiTi to assess its effect on the surface-bound redox active Ni-Ti-O material for energy storage applications.

The stress-strain response of the alloy is shown in Fig. 1c. The deformation behavior of the wire is described by elastic deformation of the austenite followed by the stress induced martensitic transformation below and up

to 5% strain. Beyond 5% strain, oriented martensites begin to deform leading to plastic deformation of oriented martensites above 15% strain. These stress induced martensites can be transformed back to austenite by heating strained wires beyond their austenitic finish (A_f) temperatures. The final mechanical strain input onto the NiTi alloy is ~8% and 11% for tensile deformations of 10% and 15% respectively, due to the intrinsic mechanical recovery of the alloy[32]. Strain recovery (10% R, 15% R) in the alloy was also measured to be ~4.5% and 3.5% respectively.

Differential scanning calorimetry (DSC) thermograms on 15% deformed and 0% deformed wires (Fig. 1d) demonstrates the transformation from stress induced martensite to parent austenite during the first heating cycle is present for the 15% tensile deformed wire in the temperature range of 50 to 60 °C whereas the unstrained (0%) wire showed no such transformations in this temperature range. This transformation during the first heating cycle is complete at a temperature of 60 °C which is the austenitic finish temperature (A_f). Based on the DSC results, the 15% and 10% tensile deformed alloy was heated to 60 °C in vacuum to complete the reverse transformation from stress induced martensitic state to parent austenite state. The transformation temperature around 60 °C is ideal in the case of metal oxides to avoid annealing effects which are prevalent at higher temperatures.

Spectroscopic strain analysis

As we use mechanical strain as an input parameter on NiTi to transfer strain to a surface oxide active material, XRD and Raman spectroscopy provide insight into strain transfer that enables controlled assessment of strain effects on electrochemical measurements. To characterize the transfer of strain applied to the superelastic/shape-memory NiTi to the metal oxide nanostructured active material on the surface, Raman spectroscopy was carried out with 532 nm excitations (Fig. 2). The coupling of strain into a material will modify local stretch modes, hence enabling Raman spectroscopy as a sensitive tool for identifying strain in materials with distinct Raman modes. Similar to previous reports on heat treated NiTi alloys[33] we find the Raman spectra of the nanostructured surface oxide to exhibit a strong peak near 269 cm^{-1} attributed to the titanate mode which are the Raman active modes of $NiTiO_3$[34–37], peaks centered on 300 cm^{-1} and 342 cm^{-1} attributed to the E_g modes of $NiTiO_3$[38–41], and a peak near 454 cm^{-1} attributed to the E_g mode of rutile phase TiO_2[42,43]. Whereas shifts and mode-splitting can be observed in these peaks as a function of applied strain, statistical Raman maps over large areas of the surface (800–1000 total Raman scans in each map) were performed to quantify strain-related shifts observed in the active materials, specifically for the modes identified in Fig. 2a. Lorentzian fits were applied to these Raman modes (Fig. 2b,c) and statistically validated strain effects were isolated. Upon strain recovery, these Raman modes revert back near or toward the unstrained peak positions, indicating the correlation between the measured Raman response and strain applied on the petaled nanostructured oxide surface. Importantly, the shift and reversal of the Raman modes upon strain and strain recovery across a large-area statistical sampling of the oxide without a significant bimodal or broadening effect on the peak distributions indicates the absence of interfacial delamination as a stress relief mechanism in this material system. Furthermore, the E_g mode of $NiTiO_3$ (Fig. 2d) and TiO_2 (Fig. 2e) are observed to exhibit similar recoverable shifts in the Raman modes that can be correlated with strain and straightforwardly identified. The low intensities of the observed Ni-O stretch modes[44–46] near 508 cm^{-1} and 571 cm^{-1} prohibited quantitative analysis on these modes.

Despite the clear signature of strain deduced through Raman spectroscopy, X-ray diffraction (XRD) provides further quantitative insight. XRD measurements indicate the same trend as Raman spectroscopy, where shifts toward lower angles are observed upon strain application, with recovery leading to the opposite shift. This is specifically shown for the (012) plane of TiO_2 (Brookite) in Fig. 2f,g. To accurately determine the strain on the surface oxide using X-Ray diffractograms, Gaussian fits were applied to the obtained peaks. A standard analytical procedure was used to correlate strain to the *d*-spacing of the strained, unstrained, and recovered states given by the following equation,

$$\%\ elastic\ \ strain = \left(\frac{d_T\ \ or\ \ d_R - d_{0\%}}{d_{0\%}}\right) \times 100\%$$

where, d_T, d_R and $d_{0\%}$ represent the *d*-spacing of the tensile strained states, the recovered states and the unstrained state, respectively. This enables the strain experienced by the surface oxide to be accurately determined. The application of 10% and 15% strain to the NiTi alloy is observed to transfer ~0.04% and ~0.08% strain to the surface oxide, which can also be recovered as described in Fig. 1c. Full XRD analysis of the material is discussed in the supporting information. Strain transfer using NiTi superelastic/shapememory alloys have so far been limited to metals[17] and alloys deposited on the surface with a maximum strain transfer of 2.18% achieved for an Fe-Pt metal alloy[47,48]. The surface oxide on the NiTi alloy, being a brittle ceramic is not as ductile as metals and metal alloys, therefore experiences cracking with less than 1% applied strain[49]. Overall, strain measured at $<0.1\%$ is expected due to the stress relief through cracking of the surface oxide and strain transfer across a nanostructured-bulk interface. The oxide layer will crack until reaching a critical tensile strain where the crack density saturates and strain is further transferred to cracked islands to "lock in" elastic strain on the surface oxide[50]. This critical tensile strain for crack density saturation is modulated by both the thickness of the oxide layer as well as morphology of the nanostructured surface oxide. As 10% and 15% strain applied to the NiTi alloy exceeds the critical tensile strain for the thick oxide layer these measurements are carried out in a regime where increased strain on the NiTi will lead to increased strain on the oxide layer, which can be experimentally studied through Raman and XRD measurements. Moreover, XRD and Raman spectroscopy provide a combined toolset that can together identify the signature of elastic strain locked in a metal or metal oxide crystal structure to impact electrochemical behavior[17]. Combined with the versatility of superelastic/shape memory NiTi materials, this provides the ideal platform for assessing and understanding the mechano-electrochemical response of the surface oxide.

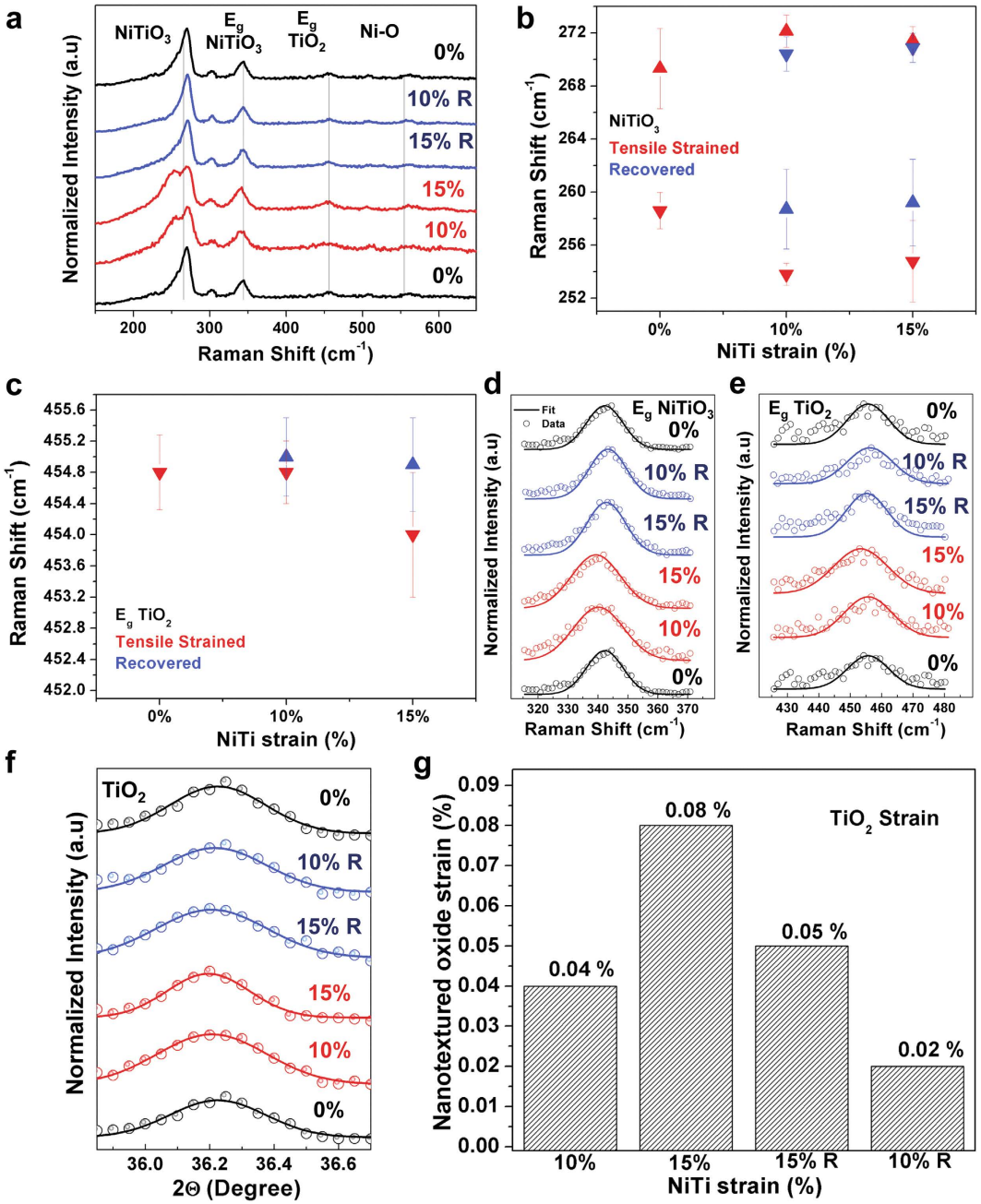

Figure 2. Characterizing strain on redox active nanostructures. (**a**) Raman spectra of the strained (10% and 15%), unstrained (0%) and recovered (10% R and 15% R) states. (**b,c**) Raman maps based on 800–1000 individual scans showing average strain effect on titanate-$NiTiO_3$ (**b**) and TiO_2 (**c**) active materials. (**d,e**) Selected spectra and the fitted curves of (**d**) E_g mode of $NiTiO_3$ and (**e**) E_g mode of TiO_2 at various strained and recovered states. (**f**) Selected X-Ray diffraction spectra and Gaussian fits of the peak corresponding to (012) plane of TiO_2 (brookite) at various strained and recovered states. (**g**) Percent strain corresponding to (**f**) based on both strained and recovered states. Note classifications of 10% and 15% strain correspond to strain applied to NiTi only.

Strain engineered electrochemistry

To characterize the effect of quantifiable strain on electrochemical performance, we build on the principle that Ni-Ti-O based oxide is active for the redox reaction with OH^- ions in alkaline electrolyte solutions[33,51,52]. Due to the ability to strain set conductive NiTi alloys, this provides an excellent platform for characterizing the role of strain transferred to the active Ni-Ti-O containing surface oxide layer on the observed redox couple in alkaline electrolytes. Cyclic Voltammetry (CV) was carried out using 2M NaOH electrolyte in a 3-electrode configuration with a Saturated Calomel Electrode (SCE) reference and a platinum counter electrode at scan rates of 100 mV/s. As previous studies have demonstrated the stability of the SCE reference electrode to address the electrochemical response of NiO, $Ni(OH)_2$, and Ni-Ti-O based metal oxides in alkaline solutions, it was chosen as the reference

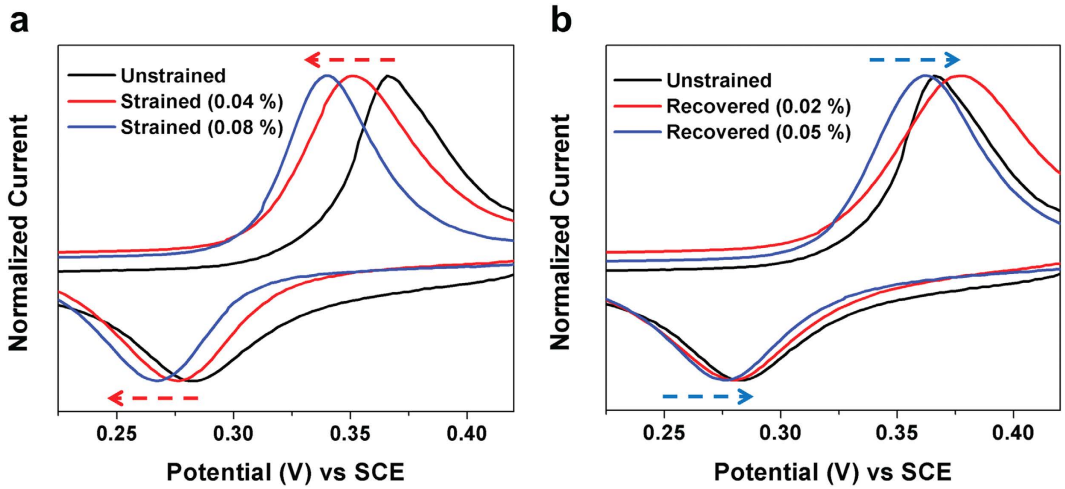

Figure 3. Correlating strain to electrochemical response. (**a**) Cyclic voltammograms with normalized current densities of the unstrained and the tensile strained (0.04%) and (0.08%) states based on surface oxides at a voltage window of 0.2 to 0.45 V. (**b**) Cyclic voltammograms with normalized current densities of the unstrained and recovered (0.02%) and (0.05%) states based on surface oxides at a voltage window of 0.2 to 0.45 V at scan rate of 100 mV/s.

electrode for the electrochemical tests[51,53–55]. (Figure 3) For purposes of comparison, the current densities were normalized to analyze the potential shifts in the anodic and cathodic branches. To accurately measure the redox peak potentials and exclude other possible sources of errors, 100 CV sweeps at a scan rate of 100 mV/s were performed within the operating voltage window to obtain reproducible voltammograms. To ensure accuracy, Gaussian fits were applied to the anodic and cathodic peaks to measure the peak potentials. CV curves comparing redox performance for both (1) different amounts of total strain applied to the surface-bound NiO-TiO_2 materials (Fig. 3a) and (2) the same materials except with the strain recovered in a manner consistent with Fig. 1c (Fig. 3b) elucidate the principle that strain has an evident and reversible effect on the voltage of the redox couple. In the first case, the shift of both the anodic and cathodic peaks toward lower potentials indicates that the observed effect is not explained by resistance or activation polarization in the electrode. The strain-induced modification to the redox energetics is further highlighted by experiments where the strain on the NiO-TiO_2 based active material can be partially recovered, leading to a shift of both the anodic and cathodic peaks toward the native potential of the redox couple measured in the unstrained material. The observation that strain recovery of the (strained) active material leads to reversal of shifts in the electrochemical response associated with strain supports key ideas: (1) it mitigates the role of other phenomena in the electrochemical potential shifts, since the electrolytes, reference electrode, and testing conditions are otherwise invariant in these tests, and (2) supports the integrity of the NiTi-oxide interface, since delamination effects under strain applied to the NiTi would inhibit further strain transfer or recovery and would expose the NiTi material to the electrolyte leading to no measureable electrochemical material response. These results suggest for the first time that mechanical strain as an input parameter can modify or control electrochemical reduction potentials relevant to metal oxide based energy storage materials. Whereas previous recent reports have indicated the effect of strain on catalysis[16,17,56–58], our results are both consistent with these reports, but with key differences. Similar to a catalytic system where charge-transfer reactions are confined to a surface, reduction and oxidation reactions contributing to the pseudocapacitance of NiO-TiO_2 involves surface reaction with OH^- ion from the electrolyte. Previous studies have indicated that doping effects can modify the oxidation state changes of Ni-based metal oxides[59–61] where equilibrium redox potential (E_{eq}) shifts can be attributed to structural distortions from doping[59]. In our study, we demonstrate mechanical strain as an input parameter, verified by XRD and Raman spectroscopy, where the local distortions of the surface oxide facilitate insertion of the OH^- ion into the surface oxide layer. This is distinguished from shifts in E_{eq} due to electrolyte concentration, heating, or modification of reference potentials since strain application and strain recovery trigger and reverses shifts in E_{eq} while electrolyte, reference electrode, and testing conditions are invariant. This is enabled by taking advantage of the shapememory response of NiTi alloy to recover the structural distortions imposed by the applied tensile strain on the surface oxides, which in turn recovers the electrochemical response. In all cases, we observe that tensile strain lowers the equilibrium redox potential associated with the physical insertion of anions to store energy in the NiO-TiO_2-based material in a manner that correlates with the total amount of applied strain (Fig. 4a and supporting information, Fig. S8). This change in reduction potential can be reversed by recovering the strain imposed in the material. As only elastic strains have the ability to simultaneously affect Raman modes, lattice spacing, and electrochemical behavior, the NiTi platform provides a versatile substrate for locking such strains in metal oxides deposited on the surface.

Based on these observations, we propose a simple concept to describe this effect that is illustrated in Fig. 4b. By applying tensile strain to the nanostructured material, the total free energy of the crystal is above its equilibrium value as described through relationships between the total cohesive energy of the crystal and the lattice parameter, such as the universal binding energy relationship (UBER). As only $<0.1\%$ strain is transferred to the surface oxide

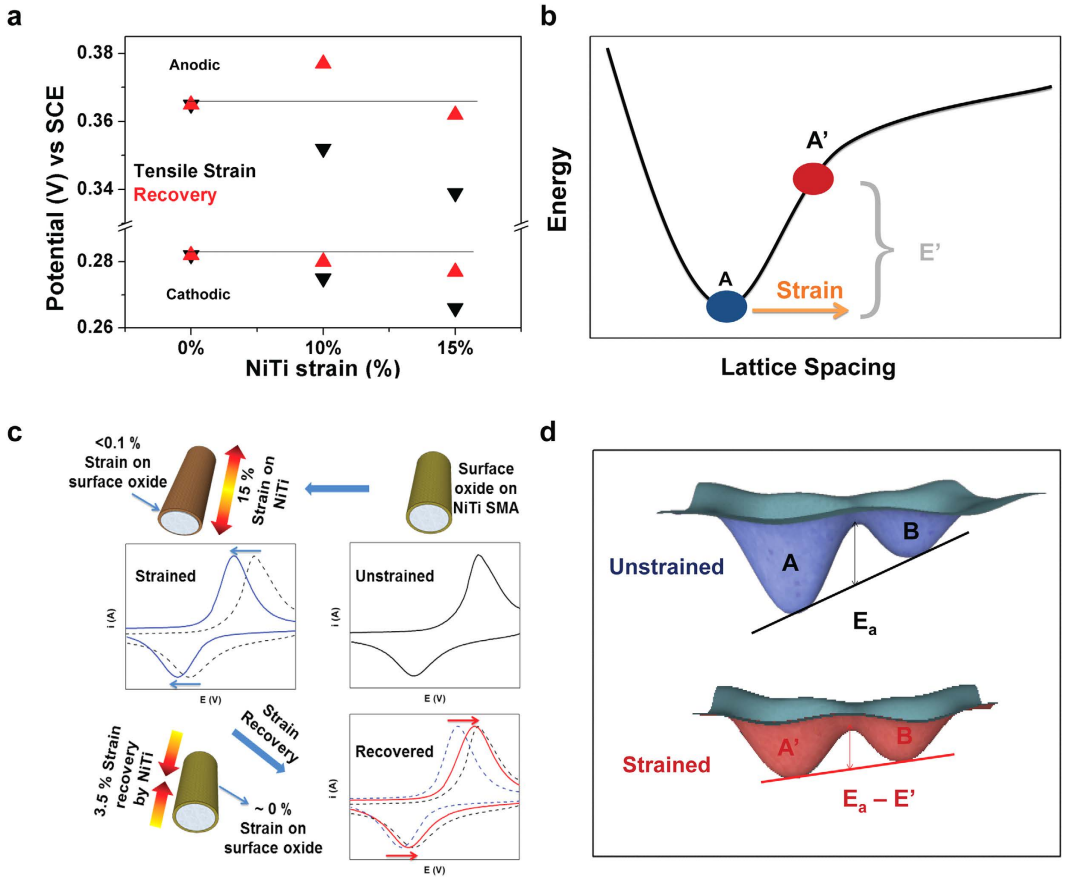

Figure 4. The role of strain to modify energy storage electrochemistry. (**a**) Anodic and cathodic peak potentials plotted versus SCE at various unstrained, strained, and recovered states of the NiTi alloy. (**b**) General plot of the total cohesive energy as a function of lattice spacing with energy difference E′ in tensile strained state that facilitates anion insertion. (**c**) Scheme representing the unstrained, strained, and recovered states of the NiTi alloy and the transferred strains on the surface oxide resulting in redox potential shifts. (**d**) Potential well representation of the transition between these states for electrochemical processes with E′ for the strained state schematically illustrated in panel (**b**).

even though the alloy undergoes 15% tensile strain, the reversible effects observed in electrochemical measurements (Fig. 4c) originate from the changes in the energy landscape of the surface oxide. Since this process requires the insertion of an anionic species into the host lattice, accompanied by an oxidation state change in the metal oxide, the increase in free energy facilitates a smaller energy barrier between the strained metal oxide (A′) and the inserted state (B) in comparison to the unstrained metal oxide (A) and the inserted state (B). This is visually represented through a potential well diagram shown in Fig. 4d. This process is distinguished from that described in electrocatalytic reactions, since effects in such systems are likely to be minimal until the imposed strain is of a significant magnitude to modify the electronic band structure of the catalytic material. Even in the case of applied strain at $<0.1\%$, our results indicate a marked effect of strain on electrochemical redox reactions relevant to redox-based energy storage systems that could be a critical tool in the future vision of engineered materials for advanced energy storage systems. Moreover, the strain can be applied to the surface oxide and be reversed to varying degrees based on the extent of preloading, thickness of the surface oxide, and anchoring to the NiTi surface which leads to isolation of mechano-electrochemical effects of energy storage redox active materials owing to the fact that the only parameter capable of reversing redox potential shifts based on this system are the mechanical strains present in the surface oxides. Also, transformational structural distortions that accompany ion insertion into metal oxide lattices during electrochemical reactions in pseudocapacitors and batteries can be studied using the NiTi platform. This would offer a control knob that can directly tailor energy landscape of existing energy storage materials.

Conclusion

In summary, we demonstrate the ability to leverage strain engineering to modify the electrochemical potential of Ni-based metal oxide nanostructures fabricated on the surface of superelastic/shape memory NiTi materials during OH^- insertion and extraction. With less than 0.1% strain, we observe shifts in the electrochemical potential up to ~30 mV. Notably, this effect is uniquely correlated with strain as the reversal of strain in the material (a feature enabled by the superelastic NiTi) leads to a subsequent recovery of the electrochemical potential shifts. This elucidates the strain tensor as a six-dimensional framework to modify the electrochemical response of

materials, opens a new area where foundational principles of electrochemistry (such as the Nernst potential) can intersect mechanical properties of materials, and provides a practical framework for improving the function of energy storage materials. As pairing of anodic and cathodic potentials dictate the total energy density of a battery, strain could potentially open a route to improve energy storage performance of batteries building from already existing materials, instead of engaging new synthesis driven routes toward new materials. Unlike semiconductor manufacturing routes that leverage strain engineering to modulate electronic properties of materials, we propose electrochemistry to be more amenable to strain engineering since both the electronic properties of a material and the physical insertion and storage of ions in a material are attributes that can be controlled with strain, as we discuss in this work.

Experimental Methods

Aging of NiTi superelastic wire. NiTi superelastic wires (0.5 mm diameter, 55% Ni from Nitinol Devices & Components, Inc.) were repeatedly sonicated for 10 min in Acetone (Aldrich) followed by Ethanol (Aldrich) and then nanopure water (Millipore water purifier). The wires were dried in air and were subjected to aging process by heating them to about 600 °C for 1 hour under vacuum with a small controlled flow of air. This led to the formation of a ~200 nm mixed oxide layer on the surface of the wires. The aging process was used to perform two functions; the activation of the superelastic/shapememory capability of the NiTi wire and to grow a thin oxide layer on the surface of the wire.

Strain setting the surface oxide. The NiTi superelastic wires were subjected to tensile deformation up to 10% and 15% strains at a rate of 2 mm/min using an Instron 5944 mechanical testing system. The unstrained (0%) and the tensile deformed (10% and 15%) wires were subjected to sonication treatment for 30 min in 30% peroxide solution to impart nanotexturing on the oxide surface and to electrochemically activate the surface oxide layer. The treated wires were rinsed in nanopure water followed by drying in air.

Differential Scanning Calorimetry. Differential Scanning Calorimetry (DSC, TA Instruments) was performed on the unstrained and strained wires to understand the strain recovery property of the alloy. The unstrained and strained wires were heated from room temperature to 100 °C in the first heating cycle followed by cooling to −100 °C in the cooling cycle and equilibrating at these respective temperatures for 5 min in aluminum pans. The subsequent heating cycle was from −100 °C to 100 °C followed by cooling. After two heating and cooling cycles the wires were equilibrated at room temperature.

Electron Imaging. Characterization of the microstructure and Energy Dispersive Spectroscopy analysis was performed using a Zeiss Merlin SEM at various magnifications using 5 KV beam voltage for imaging and 20 KV beam voltage for EDS elemental analysis. Characterization of the nanostructure of the surface oxide was performed using FEI Tecnai Osiris TEM using a 200 kV S/TEM system. STEM EDS maps were obtained on an oxide flake scrapped off from the surface of the NiTi wire to further characterize the composition of the surface oxide.

Raman and XRD characterization. Raman spectroscopy measurements were carried out using a Reinshaw Raman microscope using 532 nm Laser excitations. Maps comprising of 800–1000 spots across the surface of the wire was obtained with 60s exposure time at 10% laser power to yield a statistical strain distribution of the strained surface oxide layer. Mean peak shift corresponding to various Raman active modes of the surface oxide was obtained by using Lorrentzian fits on the obtained spectra. XRD measurements were carried out using a Scintag XGEN 4000 using Cu Kα 1.542 A°. To yield good X-Ray counts, 40 sec exposure times per 0.2 degree increments were maintained throughout the measurement.

Electrochemical Measurements. Electrochemical measurements were performed using a 3 electrode configuration in a beaker type cell with the NiTi alloy with surface oxide as the working electrode, a platinum foil (Alfa Aesar 1 cm × 1 cm) as the counter electrode and a Saturated Calomel Electrode (SCE) as the reference electrode. The electrolyte used was a 2 M NaOH solution. Cyclic voltammograms were obtained for all the unstrained and strained states of the surface oxides at a scan rate of 100 mV/s in the voltage range of 0 V to 0.5 V. All the samples were cycled for a 100 cycles at 100 mV/s to get reproducible voltammograms. All electrochemical data was normalized to the immersed area of the wire electrodes.

Strain Recovery and Analysis. The strain recovery was performed by heating the strained wires with strained surface oxides to 60 °C in a Quartz CVD tube furnace under vacuum for 1min. Due to the recovery process the strain imposed on the wire and the oxide was recovered. The change in the wire length after the recovery process was used to estimate the strain recovery by the NiTi alloy. Raman and XRD measurements were performed on the strain recovered to study the recovered strain state of the surface oxide followed by electrochemical testing using the same conditions as the unstrained and strained wires.

References

1. Arico, A. S., Bruce, P., Scrosati, B., Tarascon, J.-M. & Van Schalkwijk, W. Nanostructured materials for advanced energy conversion and storage devices. *Nat. Mater.* **4,** 366–377 (2005).
2. Larcher, D. & Tarascon, J. Towards greener and more sustainable batteries for electrical energy storage. *Nat. Chem*. **7,** 19–29 (2015).
3. Jain, A., Hautier, G., Ong, S. P., Dacek, S. & Ceder, G. Relating voltage and thermal safety in Li-ion battery cathodes: a high-throughput computational study. *Phys. Chem. Chem. Phys*. **17,** 5942–5953 (2015).
4. Mo, Y., Ong, S. P. & Ceder, G. Insights into Diffusion Mechanisms in P2 Layered Oxide Materials by First-Principles Calculations. *Chem. Mater.* **26,** 5208–5214 (2014).
5. Fu, X. *et al.* Tailoring Exciton Dynamics by Elastic Strain-Gradient in Semiconductors. *Adv. Mater.* **26,** 2572–2579 (2014).
6. Feng, J., Qian, X., Huang, C.-W. & Li, J. Strain-engineered artificial atom as a broad-spectrum solar energy funnel. *Nat. Photonics* **6,** 866–872 (2012).

7. Eres, G. *et al.* Cooperative Island Growth of Large-Area Single-Crystal Graphene on Copper Using Chemical Vapor Deposition. *ACS nano* **8,** 5657–5669 (2014).
8. Li, H. *et al.* Optoelectronic crystal of artificial atoms in strain-textured molybdenum disulphide. *Nat. Commun.* **6,** 7381 (2015).
9. Li, H. *et al.* Activating and optimizing MoS2 basal planes for hydrogen evolution through the formation of strained sulphur vacancies. *Nat. Mater.* **15,** 48–53 (2016).
10. Bissett, M. A., Tsuji, M. & Ago, H. Strain engineering the properties of graphene and other two-dimensional crystals. *Phys. Chem. Chem. Phys.* **16,** 11124–11138 (2014).
11. Lu, J., Neto, A. C. & Loh, K. P. Transforming moiré blisters into geometric graphene nano-bubbles. *Nat. Commun.* **3,** 823 (2012).
12. Liu, Z. *et al.* Strain and structure heterogeneity in MoS2 atomic layers grown by chemical vapour deposition. *Nat. Commun.* **5,** 5246 (2014).
13. Wang, L. *et al. In situ* atomic-scale observation of continuous and reversible lattice deformation beyond the elastic limit. *Nat. Commun.* **4,** 2413 (2013).
14. Wang, L., Zhang, Z. & Han, X. *In situ* experimental mechanics of nanomaterials at the atomic scale. *NPG Asia Mater.* **5,** e40 (2013).
15. Gong, M., Jin, X., Sakidja, R. & Ren, S. Synergistic strain engineering effect of hybrid plasmonic, catalytic and magnetic core-shell nanocrystals. *Nano Lett.* **15,** 8347–8353 (2015).
16. Kibler, L. A., El-Aziz, A. M., Hoyer, R. & Kolb, D. M. Tuning reaction rates by lateral strain in a palladium monolayer. *Angew. Chem. Int. Ed. Engl.* **44,** 2080–2084 (2005).
17. Du, M., Cui, L., Cao, Y. & Bard, A. J. Mechanoelectrochemical Catalysis of the Effect of Elastic Strain on a Platinum nanofilm for the ORR Exerted by a Shape Memory Alloy Substrate. *J. Am. Chem. Soc.* **137,** 7397–7403 (2015).
18. Sneed, B. T., Young, A. P. & Tsung, C.-K. F. Building Up Strain in Colloidal Metal Nanoparticle Catalysts. *Nanoscale* **7,** 12248–12265 (2015).
19. Amakawa, K. *et al.* How Strain Affects the Reactivity of Surface Metal Oxide Catalysts. *Angew. Chem. Int. Ed. Engl.* **52,** 13553–13557 (2013).
20. Aidhy, D. S. *et al.* Fast ion conductivity in strained defect-fluorite structure created by ion tracks in Gd2Ti2O7. *Sci. Rep.* **5,** 16297 (2015).
21. Han, J. W. & Yildiz, B. Enhanced one dimensional mobility of oxygen on strained LaCoO 3 (001) surface. *J. Mater. Chem.* **21,** 18983–18990 (2011).
22. Tsvetkov, N., Lu, Q., Chen, Y. & Yildiz, B. Accelerated Oxygen Exchange Kinetics on Nd2NiO4+ δ Thin Films with Tensile Strain along c-Axis. *ACS Nano* **9,** 1613–1621 (2015).
23. Kim, S. *et al.* Electrochemically driven mechanical energy harvesting. *Nat. Commun.* **7,** 10146 (2016).
24. Simon, P. & Gogotsi, Y. Materials for electrochemical capacitors. *Nat. Mater.* **7,** 845–854 (2008).
25. Sheldon, B. W., Soni, S. K., Xiao, X. & Qi, Y. Stress contributions to solution thermodynamics in Li-Si alloys. *Electrochem. Solid State Lett.* **15,** A9–A11 (2011).
26. Chon, M. J., Sethuraman, V. A., McCormick, A., Srinivasan, V. & Guduru, P. R. Real-time measurement of stress and damage evolution during initial lithiation of crystalline silicon. *Phys. Rev. Lett.* **107,** 045503 (2011).
27. Zeng, Z. *et al. In situ* measurement of lithiation-induced stress in silicon nanoparticles using micro-Raman spectroscopy. *Nano Energy* **22,** 105–110 (2016).
28. Azizi, A. *et al.* Dislocation motion and grain boundary migration in two-dimensional tungsten disulphide. *Nat. Commun.* **5,** 4867 (2014).
29. Liu, Y., Merinov, B. V. & Goddard, W. A. Origin of low sodium capacity in graphite and generally weak substrate binding of Na and Mg among alkali and alkaline earth metals. *Proc. Natl. Acad. Sci. USA* **113,** 3735–3739 (2016).
30. Hansen, A. W. *et al.* Oxide Formation on NiTi Surface: Influence of the Heat Treatment Time to Achieve the Shape Memory. *Materials Research* **18,** 1053–1061 (2015).
31. Firstov, G., Vitchev, R., Kumar, H., Blanpain, B. & Van Humbeeck, J. Surface oxidation of NiTi shape memory alloy. *Biomaterials* **23,** 4863–4871 (2002).
32. Tan, G., Liu, Y., Sittner, P. & Saunders, M. Lüders-like deformation associated with stress-induced martensitic transformation in NiTi. *Scr. Mater.* **50,** 193–198 (2004).
33. Liu, Q., Ding, D. & Ning, C. Anodic Fabrication of Ti-Ni-O Nanotube Arrays on Shape Memory Alloy. *Materials* **7,** 3262–3273 (2014).
34. Santara, B., Giri, P., Imakita, K. & Fujii, M. Evidence of oxygen vacancy induced room temperature ferromagnetism in solvothermally synthesized undoped TiO2 nanoribbons. *Nanoscale* **5,** 5476–5488 (2013).
35. Kim, S.-J. *et al.* Characterization of hydrothermally prepared titanate nanotube powders by ambient and *in situ* Raman spectroscopy. *J. Phys. Chem. Lett.* **1,** 130–135 (2009).
36. Bellat, V. *et al.* A multi-step mechanism and integrity of titanate nanoribbons. *Dalton Trans.* **44,** 1150–1160 (2015).
37. Byrne, M. T. *et al.* Chemical functionalisation of titania nanotubes and their utilisation for the fabrication of reinforced polystyrene composites. *J. Mater. Chem.* **17,** 2351–2358 (2007).
38. Baraton, M., Busca, G., Prieto, M., Ricchiardi, G. & Escribano, V. S. On the vibrational spectra and structure of FeCrO3 and of the ilmenite-type compounds CoTiO3 and NiTiO3. *J. Solid State Chem.* **112,** 9–14 (1994).
39. GallardoáAmores, J. M. & SanchezáEscribano, V. FT Raman and FTIR studies of titanias and metatitanate powders. *J. Chem. Soc. Faraday Trans.* **90,** 3181–3190 (1994).
40. Nguyen-Phan, T.-D., Huy, C. N., Kim, C.-K. & Shin, E. W. Facile microwave-assisted synthesis and controllable architecture of three-dimensional nickel titanate. *CrystEngComm* **17,** 4562–4574 (2015).
41. Bellam, J. B. *et al.* Visible-light photocatalytic activity of nitrogen-doped NiTiO3 thin films prepared by a co-sputtering process. *RSC Adv.* **5,** 10551–10559 (2015).
42. Yan, J. *et al.* Understanding the effect of surface/bulk defects on the photocatalytic activity of TiO2: anatase versus rutile. *Phys. Chem. Chem. Phys.* **15,** 10978–10988 (2013).
43. Li, L. *et al.* Sub-10 nm rutile titanium dioxide nanoparticles for efficient visible-light-driven photocatalytic hydrogen production. *Nat. Commun.* **6,** 5881 (2015).
44. Zhou, M., Chai, H., Jia, D. & Zhou, W. The glucose-assisted synthesis of a graphene nanosheet–NiO composite for high-performance supercapacitors. *New J. Chem.* **38,** 2320–2326 (2014).
45. Lu, M.-L., Lin, T.-Y., Weng, T.-M. & Chen, Y.-F. Large enhancement of photocurrent gain based on the composite of a single n-type SnO2 nanowire and p-type NiO nanoparticles. *Opt. Express* **19,** 16266–16272 (2011).
46. Luo, C., Li, D., Wu, W., Zhang, Y. & Pan, C. Preparation of porous micro–nano-structure NiO/ZnO heterojunction and its photocatalytic property. *RSC Adv.* **4,** 3090–3095 (2014).
47. Feng, C. *et al.* Nonvolatile modulation of electronic structure and correlative magnetism of L10-FePt films using significant strain induced by shape memory substrates. *Sci. Rep.* **6,** 20199 (2016).
48. Feng, C. *et al.* Reversible and Nonvolatile Modulations of Magnetization Switching Characteristic and Domain Configuration in L10-FePt Films via Nonelectrically Controlled Strain Engineering. *ACS Appl. mater. Interfaces* **8,** 7545–7552 (2016).
49. Racek, J. *et al.* Monitoring Tensile Fatigue of Superelastic NiTi Wire in Liquids by Electrochemical Potential. *Shap. Mem. Superelasticity* **1,** 204–230 (2015).

50. Jen, S.-H., Bertrand, J. A. & George, S. M. Critical tensile and compressive strains for cracking of Al2O3 films grown by atomic layer deposition. *J. Appl. Phys.* **109,** 084305 (2011).
51. Hang, R. *et al.* Fabrication of Ni-Ti-O nanotube arrays by anodization of NiTi alloy and their potential applications. *Sci. Rep*. **4,** 7547 (2014).
52. Gao, Z.-D., Han, Y., Wang, Y., Xu, J. & Song, Y.-Y. One-step to prepare self-organized nanoporous NiO/TiO2 layers and its use in non-enzymatic glucose sensing. *Sci. Rep*. **3,** 3323 (2013).
53. Li, H. *et al.* Amorphous nickel hydroxide nanospheres with ultrahigh capacitance and energy density as electrochemical pseudocapacitor materials. *Nat. Commun.* **4,** 1894 (2013).
54. Zhu, Y. *et al.* Ultrathin nickel hydroxide and oxide nanosheets: synthesis, characterizations and excellent supercapacitor performances. *Sci. Rep.* **4,** 5787 (2014).
55. Gu, Y. *et al.* NiTi layered double hydroxide thin films for advanced pseudocapacitor electrodes. *J. Mater. Chem.* **1,** 10655–10661 (2013).
56. Stamenkovic, V. *et al.* Changing the activity of electrocatalysts for oxygen reduction by tuning the surface electronic structure. *Angew. Chem.* **118,** 2963–2967 (2006).
57. Strasser, P. *et al.* Lattice-strain control of the activity in dealloyed core–shell fuel cell catalysts. *Nat. Chem*. **2,** 454–460 (2010).
58. Svedruzic, D. & Gregg, B. A. Mechano-Electrochemistry and Fuel-Forming Mechano-Electrocatalysis on Spring Electrodes. *J. Phys. Chem. C* **118,** 19246–19251 (2014).
59. Lee, H. J., Lee, J. H., Chung, S. Y. & Choi, J. W. Enhanced Pseudocapacitance in Multicomponent Transition-Metal Oxides by Local Distortion of Oxygen Octahedra. *Angew. Chem.* **55,** 1–6 (2016).
60. Wang, Q., Liu, S., Sun, H. & Lu, Q. Synthesis of a flower-like Co-doped Ni (OH)2 composite for high-performance supercapacitors. *RSC Adv*. **5,** 48181–48186 (2015).
61. Hu, G. *et al.* The sol-gel-derived nickel-cobalt oxides with high supercapacitor performances. *J. Electrochem. Soc.* **158,** A695–A699 (2011).

Acknowledgements

We thank Bradly Baer for assistance in strain measurements, Dr. Leon Bellan for generous use of facilities in his laboratory for strain setting, Dr. Rizia Bardhan for use of the Raman microscope for strain analysis, Timothy Boire for his guidance during DSC measurements, and Alice Leach for assistance with XRD. We also thank Andrew Westover, Anna Douglas, Keith Share, and Mengya Li for useful discussions. This work was supported by an NSF graduate research fellowship (A.P.C.) number 1445197 and Vanderbilt University start-up funds.

Author Contributions

N.M. and C.L.P. jointly conceived the project and designed the experiments. N.M. performed material fabrication with insights from R.C., A.P.C. and L.O. and carried out mechanical and electrochemical testing and XRD analysis. N.M. carried out the Raman map analysis with insights from A.P.C. and R.C. performed SEM imaging and analysis. N.M. and C.L.P. wrote the manuscript and all authors participated in discussion and revisions to the manuscript prior to submission.

Additional Information

Supplementary information accompanies this paper at http://www.nature.com/srep

Competing financial interests: The authors declare no competing financial interests.

How to cite this article: Muralidharan, N. *et al.* Strain Engineering to Modify the Electrochemistry of Energy Storage Electrodes. *Sci. Rep.* **6**, 27542; doi: 10.1038/srep27542 (2016).